separations

Article

Application of the Fourier Transform to Improve the Accuracy of Gamma-Based Volume Percentage Detection System Independent of Scale Thickness

Abdulilah Mohammad Mayet [1], John William Grimaldo Guerrero [2,*], Thafasal Ijyas [1], Javed Khan Bhutto [1], Neeraj Kumar Shukla [1], Ehsan Eftekhari-Zadeh [3,*] and Hala H. Alhashim [4]

[1] Electrical Engineering Department, King Khalid University, Abha 61411, Saudi Arabia; amayet@kku.edu.sa (A.M.M.); ithafasal@kku.edu.sa (T.I.); jbhutto@kku.edu.sa (J.K.B.); nshukla@kku.edu.sa (N.K.S.)
[2] Department of Energy, Universidad de la Costa, Barranquilla 080001, Colombia
[3] Institute of Optics and Quantum Electronics, Friedrich Schiller University Jena, Max-Wien-Platz 1, 07743 Jena, Germany
[4] Department of Physics, College of Science, Imam Abdulrahman Bin Faisal University, Dammam 31441, Saudi Arabia; halhashim@iau.edu.sa
* Correspondence: jgrimald1@cuc.edu.co (J.W.G.G.); e.eftekharizadeh@uni-jena.de (E.E.-Z.)

Abstract: With the passage of time, scale gradually forms inside the oil pipeline. The produced scale, which has a high density, strongly attenuates photons, which lowers the measurement accuracy of three-phase flow meters based on gamma radiation. It is worth mentioning that the need for multiphase flow metering arises when it is necessary or desirable to meter well stream(s) upstream of inlet separation and/or commingling. In this investigation, a novel technique based on artificial intelligence is presented to overcome the issue mentioned earlier. Initially, a detection system was comprised of two NaI detectors and a dual-energy gamma source (241 Am and 133 Ba radioisotopes) using Monte Carlo N particle (MCNP) code. A stratified flow regime with varying volume percentages of oil, water, and gas was modeled inside a pipe that included a scale layer with varying thicknesses. Two detectors record the attenuated photons that could travel through the pipe. Four characteristics with the names of the amplitude of the first and second dominant signal frequencies were extracted from the received signals by both detectors. The aforementioned obtained characteristics were used to train two Radial Basis Function (RBF) neural networks to forecast the volumetric percentages of each component. The RMSE value of the gas and oil prediction neural networks are equal to 0.27 and 0.29, respectively. By measuring two phases of fluids in the pipe, the volume of the third phase can be calculated by subtracting the volume of two phases from the total volume of the pipe. Extraction and introduction of suitable characteristics to determine the volume percentages, reducing the computational burden of the detection system, considering the scale value thickness the pipe, and increasing the accuracy in determining the volume percentages of oil pipes are some of the advantages of the current research, which has increased the usability of the proposed system as a reliable measuring system in the oil and petrochemical industry.

Keywords: stratified flow regime; scale thickness independent; three-phase flow; RBF neural network

check for updates

Citation: Mayet, A.M.; Guerrero, J.W.G.; Ijyas, T.; Bhutto, J.K.; Shukla, N.K.; Eftekhari-Zadeh, E.; Alhashim, H.H. Application of the Fourier Transform to Improve the Accuracy of Gamma-Based Volume Percentage Detection System Independent of Scale Thickness. *Separations* **2023**, *10*, 534. https://doi.org/10.3390/separations10100534

Academic Editor: Hongbo Gu

Received: 10 August 2023
Revised: 3 September 2023
Accepted: 10 September 2023
Published: 7 October 2023

1. Introduction

In various oil fields across the world, scale buildup in pipes carrying oil has resulted in several issues. The flow of petroleum products is complicated by scale development, which decreases the pipeline's effective cross-sectional area. This component makes it impossible for pumps and other machinery to function correctly. If scale builds up in the pipeline and is not detected in time, it may lead to catastrophic breakdowns, broken oil equipment, high maintenance expenses, and decreased efficiency. For this reason, employing a control system that has characteristics such as volume percentage detection is quite helpful in advancing things when scale is present. Gamma-ray attenuation systems are frequently referred to as the gold standard by researchers when calculating the different characteristics of a polyphase flow [1–7]. A cesium source, two sodium iodide detectors, and a test pipe were utilized in the experiment described in [1]. The RBF neural network was trained with data from two detectors to provide predictions about two-phase flow parameters in the bubbly, stratified, and annular regimes. These counts were used to determine the flow regimes and make volume estimates. Roshani and his coworkers [2] used GMDH-type networks trained on the unbalanced data to predict the volume percentages and flow regime. The huge computational strain they placed on the system was justified by its extraordinary precision. In 2020, researchers utilized the MLP neural network and a single pencil beam gamma-ray attenuation technique to determine the volumetric fraction of a three-phase flow [3]. By using a cesium source, a test pipe, and a sodium iodide detector, Islami-Rad and his team were able to develop a method for precise volume percentage calculation [4]. In a recent research paper [5], the authors looked into the viability of using GMDH neural networks to determine the presence of various flow regimes and make predictions for volume fractions. While the study's volume percentage calculations were mostly accurate, they did not account for the amount of scale present in the pipe, which was a significant restriction. The flow rates were experimented with using a two-phase automated test loop in [6], which may produce various flow patterns in a horizontal channel. The measurement package setup comprised of a Cs-137 radiation source with 662 keV photon energy and a NaI (Tl) scintillation detector to count transmissions. The preferred processing component was a multi-layer perceptron (MLP). The scale layer in the oil pipe was recently measured using a dual energy source of Am-241 and Ba-133. After the simulation of three-phase flow in stratified regimes, it was established that the amplitude of the first to fourth dominant frequency should feed into the MLP neural network. The RMSE for their estimate of scale thickness was less than 0.13 [7]. Problems can arise with the use of radioisotopes as a constant power source, including those related to transportation and the requirement for personnel to wear protective gear. Therefore, X-ray tube research into measuring multiphase flow properties has gained traction of late [8–12]. In the study [8], the researchers used an X-ray tube and a NaI detector so that they could identify the volumetric percentage and regime type of two-phase flows. The timing features of the detected signals were used to train two MLP neural networks. In [9], two-phase flows were studied by modeling them in various regimes at different volume fractions. In addition, artificial neural networks were educated by feeding them the statistical features of the incoming signals. The Monte Carlo N particle (MCNP) algorithm was used to simulate four petroleum products that combined two-by-two with various quantities and were centered on the X-ray tube [10]. The signals were sent into three multilayer perceptron neural networks, which then predicted the volume ratio of the three products based on their inputs. Once the volume ratios of the first three products were established, calculating the volume ratio of the last product was a breeze. The presented method predicted the types and quantities, but was unable to reach a high degree of accuracy due to a lack of feature extraction techniques. Wavelet transformations were examined as a feature extraction approach by Balubaid et al. [11] in order to further the research [10]. One outcome of this activity was the optimization of the computational burden and the improvement of accuracy. For the modeling of a volume percentage detection system using Monte Carlo N particle (MCNP), a NaI detector and dual-energy gamma generator simulations (241 Am and 133 Ba radioisotopes) were suggested. A stratified flow regime with varying volume percentages was used to transport oil, water, and gas via a conduit with varying wall thicknesses. A detector then collected the photons that travel down the pipe after gamma rays have been released from one end. The detector measured four temporal characteristics: kurtosis, mean square root (MSR), skewness, and waveform length (WL). Two GMDH neural networks were trained using the aforementioned data to provide very accurate predictions of future volumes [12]. A 149.5 keV X-ray beam and two planar germanium detectors were used to forecast volume fractions in a three-phase system using X-ray transmission and scattering data, as described in [13]. The MCNP6 algorithm has been used to estimate fluid volume fractions for an annular flow regime. The energy spectra from both detectors were correlated with the volume percentages of the fluids using a statistical approach based on an artificial neural network. The enhancement of the hysteretic behavior with a decrease in the microchannel diameter is investigated in [14] using current monitoring measurements and finite element numerical simulations. Microchannels with internal diameters of 5 μm and 100 μm were used for the investigation, and three solution pairings were chosen: KCl-NaCl (dissimilar ionic species with similar concentration), NaCl, and KCl (identical ionic species but different concentrations), and water. The coupling effect of the wider/tighter interfacial width and the minority pH-governing ion-driven hysteresis, which was previously established to be the genesis of EOF hysteresis, causes the EOF hysteresis to increase for the decreased channel diameter (i.e., the 5 μm microchannel). With the aid of earlier research in the sector, an effort has been made in this study to offer a volume percentages diagnosis method with excellent accuracy. A three-phase flow regime with varying volume percentages of water, gas, and oil was simulated for this purpose. Each simulation took a different scale thickness value into account. An attempt was made to forecast volume percentages with good accuracy by extracting the frequency features of amplitude of the first and second dominant signals frequency received by both detectors, and putting them to two RBF neural networks. The results of this study contributed in the following areas by:

1. Enhancing the accuracy of the detecting mechanism.
2. Conducting volumetric fraction measurements of a three-phase flow as it traveled through a scale-lined oil pipe.
3. Analyzing the efficiency of the frequency characteristics in determining the volume percentages.
4. Aggregating helpful characteristics to significantly reduce the computational load.

2. Materials and Methods

2.1. Simulation Setup

Many research papers have demonstrated that academics are interested in utilizing the MCNP algorithm to model X-ray or gamma radiation-using structures [15–18]. The MCNP code simulation platform was used to mimic the framework suggested in this study [19]. Radioisotopes 241 Am and 133 Ba are at the center of the study's suggested framework. The abovementioned dual energy source shoots photons toward a steel flow channel and gathers them at the other end using two detectors. Both of its photons have energy of 59 keV and 356 keV. Two sodium iodide detectors, each 2.54 cm × 2.54 cm, are set at an angle of 0 and 7 degrees with respect to the fictitious horizon line. In the test pipe, a three-phase flow is modeled in a stratified flow regime where it takes place. The aforementioned pipe has an internal diameter of 10 cm and a thickness of 0.5 cm. There is a scale constructed of $BaSO_4$ with various thicknesses inside this pipe. Scales with density of 4.5 g per cubic centimeter with thicknesses of 0, 0.5, 1, 1.5, 2, and 3 cm were installed in the pipe through which water, oil, and gas flow. Water has a density of 1, gas has a density of 0.00125, and oil has a density of 0.826 g per cubic cm in this model. This study used the MCNP code to implement the structure. In our earlier work, we conducted multiple trials to verify the simulated structure used in this research [1]. Comparative analysis was undertaken between the detector responses obtained in the simulation and experiment. In order to compare the experimental and simulation data both were converted to units, as the Tally output in the MCNP algorithm is per source particle. The highest relative change for detector response data between real and simulated data is 2.2%. The outcomes indicate that the results of the experiment and the simulated outcomes correlate rather well. A total of 252 simulations were produced by using the 36 alternative volume percentages that are available for every 7 values of the scale thickness. In order to train the neural network, four features from each simulation—the amplitude of the first and second dominant signals frequency received by both detectors—were retrieved. There are four inputs and one output for each of the two neural networks. When combined, they provide the relative volumes of the gas and oil phases. It should be obvious that, by subtracting these two quantities from the initial total volume, the water volume percentage could be calculated. Figure 1 depicts the whole specified structure. Figure 2 presents an illustration of the recorded signals for both detectors in 1 cm scale thickness.

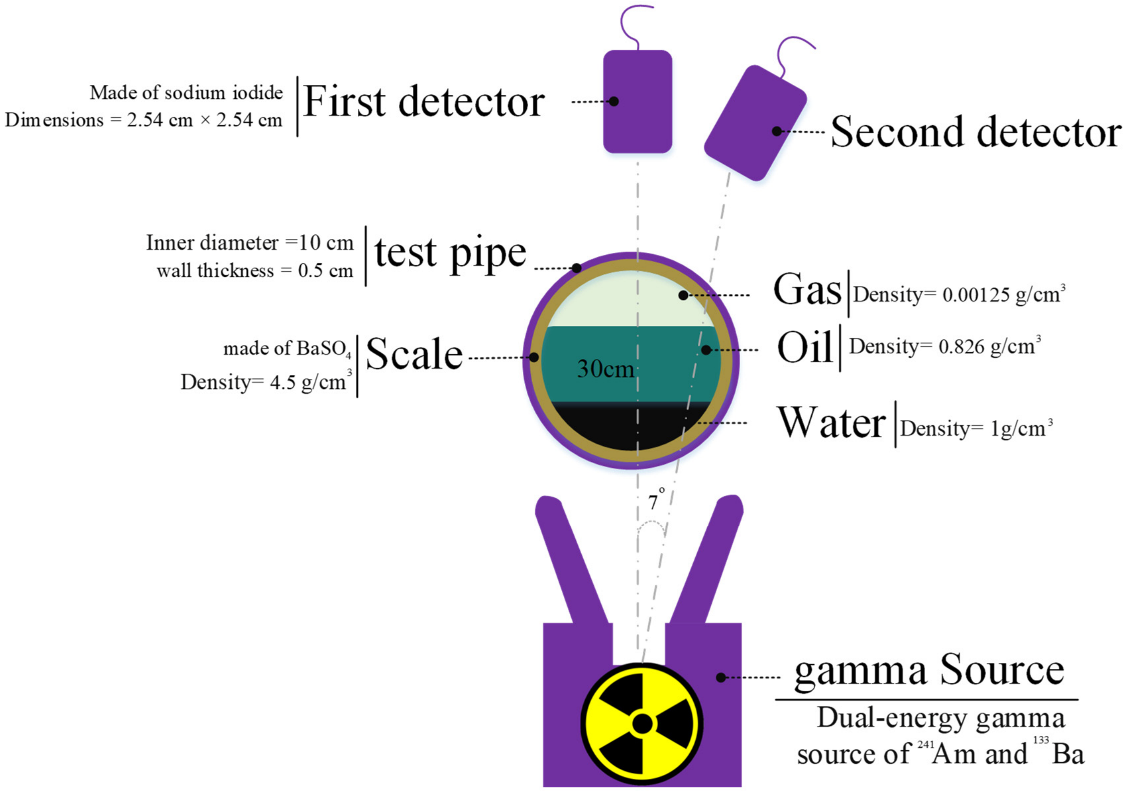

Figure 1. The simulated detecting system's architecture.

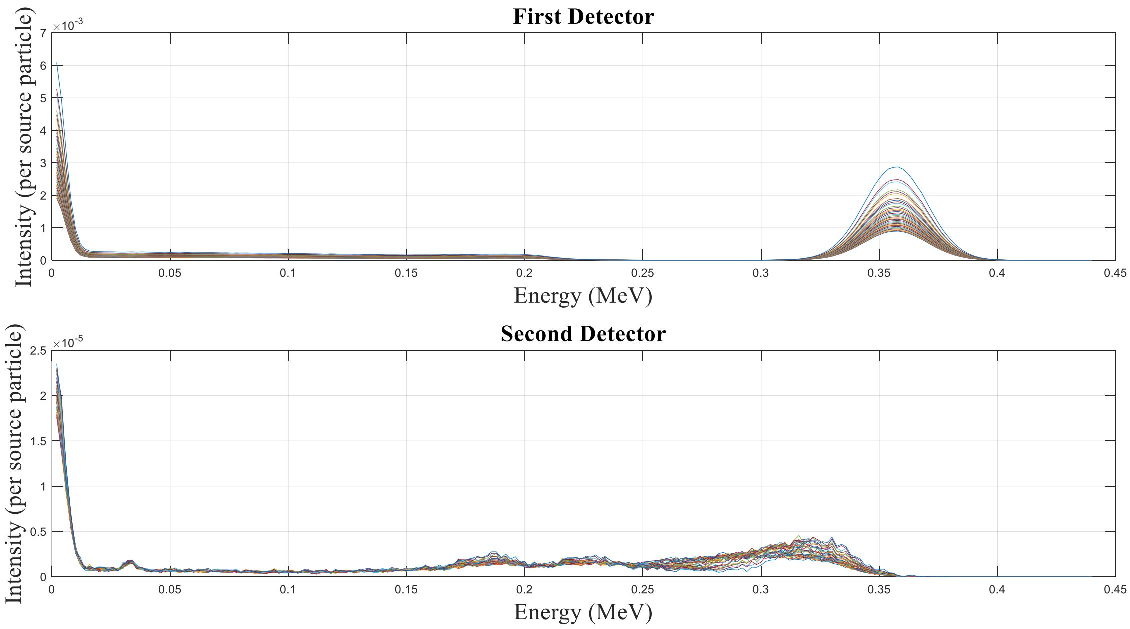

Figure 2. Signals recorded by both detectors in 1 cm scale thickness.

2.2. Feature Extraction

Feature extraction is a technique for transforming the existing data into a different domain, where machine learning-based algorithms can work more effectively. Additionally, the feature extraction method will decrease data dimensions, computation costs, and speed up machine learning methods. There are several ways to extract features. Feature extraction in the time domain, frequency domain, and time-frequency domain are several examples. The signals utilized in this study were transformed using fast Fourier transform (FFT) to make them more easily accessible for analysis in the frequency domain. Equation (1) is related to the FFT [20]. Let $x_0, \ldots,\ x_{N-1}$ be complex numbers. The DFT is defined by the formula

$$Y_k = \sum_{n=0}^{N-1} x_n e^{-i2\pi kn/N} \qquad k = 0, \ldots, N-1 \tag{1}$$

where $e^{i2\pi/N}$ is one of the n roots of unity. Each output, X_k, has to add up to N terms since there are N outputs.

Amplitude of First Dominant Frequency (AFDF) and Amplitude of Second Dominant Frequency (ASDF) were identified after analyzing the signal characteristics that were converted to the frequency domain. The diagram of a frequency domain signal is shown in Figure 3. In this graph, the x-axis indicates the frequency in Hz, the y-axis the indicates the scale's thickness in cm, and the z-axis indicates the amplitude. The characteristics that were retrieved in this stage are used as inputs into neural networks to calculate the volumetric percentages independent of scale thickness.

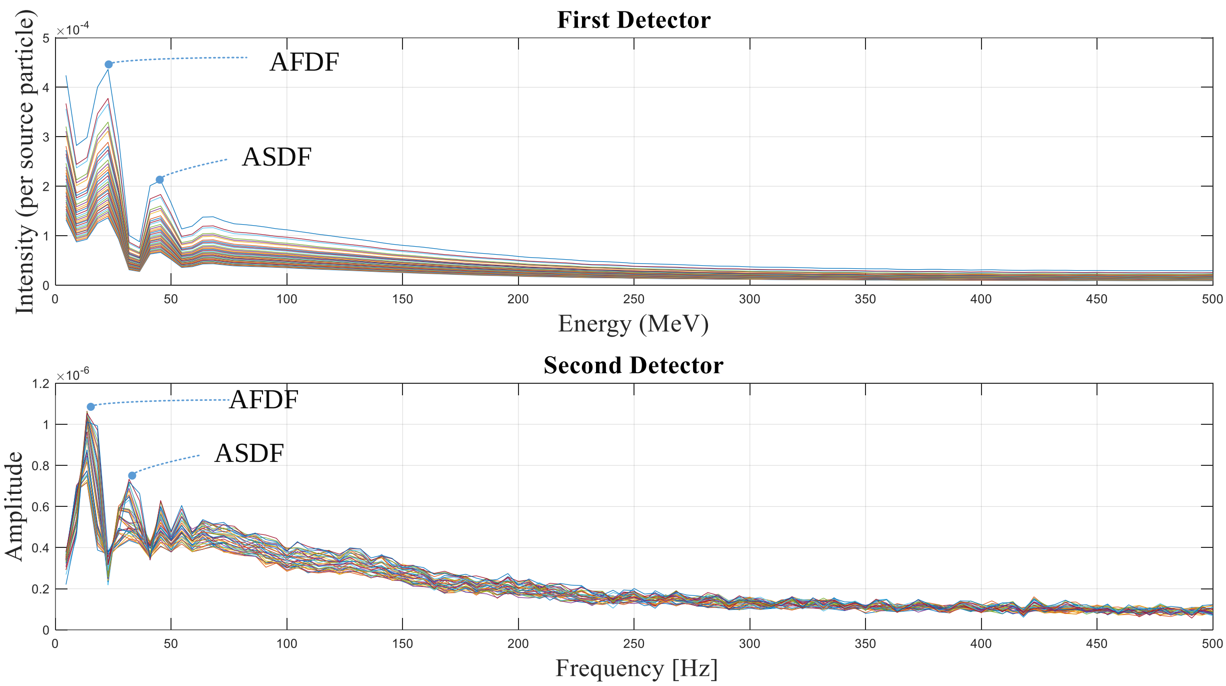

Figure 3. Extracted features for signals recorded in scale thickness of 1 cm.

2.3. Radial Basis Function Neural Network

Radial Basis Function Neural Networks (RBF NNs) are a special kind of artificial neural network that uses distance to provide estimates of data similarity. An RBF network is a kind of artificial neural network that uses the feed-forward architecture and consists of an input layer, a hidden layer, and an output layer. Radial basis functions trigger the activation of hidden layer neurons. The radial base function's most typical form is as follows [21]:

$$\varphi(r) = \exp[-\frac{r^2}{2\sigma^2}] \tag{2}$$

The distance from the cluster's center is measured in terms of a number called r. A typical bell-shaped curve is seen in Equation (2). An assortment of computational elements known as hidden nodes make up a hidden layer. A central vector c, a parametric vector with length comparable to the input vector x, is present in each concealed node. The following formula is used to determine the Euclidean distance between the network's input vector x and center vector [22]:

$$r_j = \sqrt{\sum_{i=1}^{n} (x_i - w_{ij})^2} \tag{3}$$

As a result, the following is the hidden layer's jth neuron output:

$$\varnothing_j = \exp[-\frac{\sum_{i=1}^{n} (x_i - w_{ij})^2}{2\sigma^2}] \tag{4}$$

σ is a description of the bell curve's breadth or radius. The weighted units in the hidden layer of an RBF network correspond to the vector that represents the cluster center. Traditional approaches such as the K-Mean algorithm or Kohonen algorithm-based methods can be used to determine weights. In either instance, the algorithms find the best match for the number of predicted clusters (k) when the training is performed unsupervised. The provided data are often split into training and testing data types for neural network creation. More data is present in training data—typically 70% more. The properties indicated in the preceding part were extracted using MATLAB Version: 9.13.0 (R2022b) Update 2, which was also utilized to create RBF neural networks. In this study, neural networks were not made with pre-made toolboxes. Instead, the training and testing processes were carefully coded manually to give the researchers as much freedom as possible. This MATLAB package includes a number of toolboxes for creating neural networks. It should be mentioned that the neural network was trained using the "newrb" function. The neural network design procedure started after providing the necessary inputs. In this study there are 176 training data and 76 test data. Many scholars [23–25] have been interested in the use of sophisticated mathematical techniques and artificial neural networks in a variety of scientific domains.

3. Results and Discussion

Two RBF neural networks, each taking in a 4 × 252 matrix, were trained using four features acquired from the preceding sections. Each neural network produced a 1 × 252 matrix representing the volume percentage of gas or oil. The best architectures for calculating gas and oil volumes are shown in Figures 4 and 5, respectively. Different neural networks were constructed with varying numbers of hidden layer neurons. Two RBF neural networks have been trained to determine gas and oil volume percentages. Both have four neurons in the input layer, one in the output layer, and 38 neurons and 27 in their hidden layer, respectively. Technical characteristics for these networks are shown in Table 1. Two criteria, MRE and RMSE, are proposed for determining the error value of the current networks. For these requirements the following equations are used:

$$MRE\% = 100 \times \frac{1}{N} \sum_{j=1}^{N} \left| \frac{X_j(Exp) - X_j(Pred)}{X_j(Pred)} \right| \tag{5}$$

$$RMSE = \left[\frac{\sum_{j=1}^{N} (X_j(Exp) - X_j(Pred))^2}{N} \right]^{0.5} \tag{6}$$

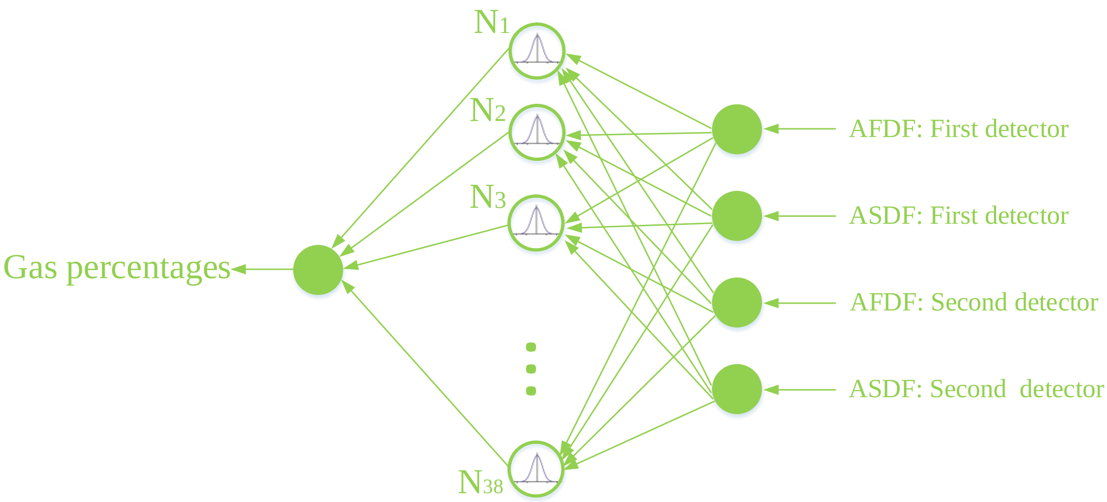

Figure 4. RBF Neural network for forecasting the proportion of gas volume.

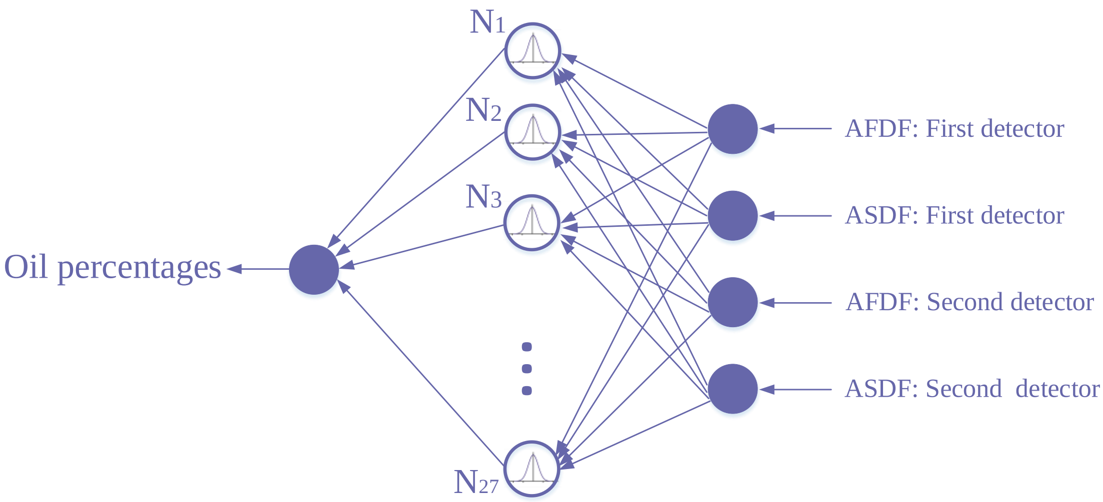

Figure 5. RBF Neural network for forecasting the proportion of oil volume.

Table 1. The RBF neural network specifications.

ANN	Gas Predictor		Oil Predictor	
Neurons in the input layer	4		4	
Neurons in the hidden layer	38		27	
Neurons in the output layer	1		1	
RBF spread	4		5	
RMSE	Train set	Test set	Train set	Test set
	0.27	0.18	0.27	0.29
MRE%	0.9	1.1	1.0	1.2

The experimental and predicted values of the ANN are denoted by "X(Exp)" and "X(Pred)", respectively, where N is the total number of observations. The obtained error is significantly lower than the previous presented method in [26], which was not equipped with the feature extraction method. In fact, in this paper a better answer than previous papers was achieved with the usage of the feature extraction method in the frequency domain, powerful artificial neural networks, and novel mathematical techniques—which is the main novelty of this work.

Training data and test data are the two categories into which the accessible data are separated. The fit diagram and error diagram in Figures 6 and 7 demonstrate how neural networks respond to these two groups. In one graph, the fitting diagram displays both the network output and desired output. To show how accurate the network is, the error diagram illustrates the discrepancy between the two target outputs and the network output. The comparison table of the output values of the neural networks and the target for two categories of training and testing data can be seen in Table 2. The comparison of the accuracy of the current research with previous research can be seen in Table 3.

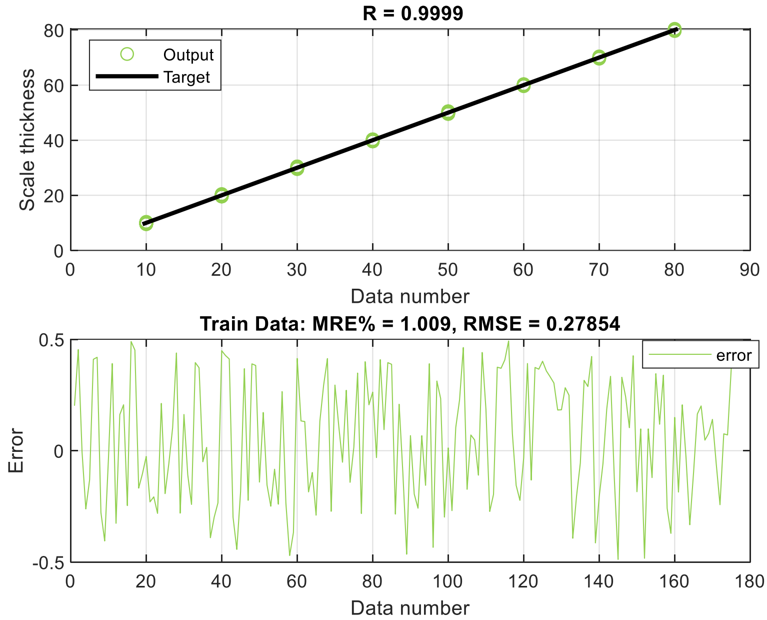

(**a**)

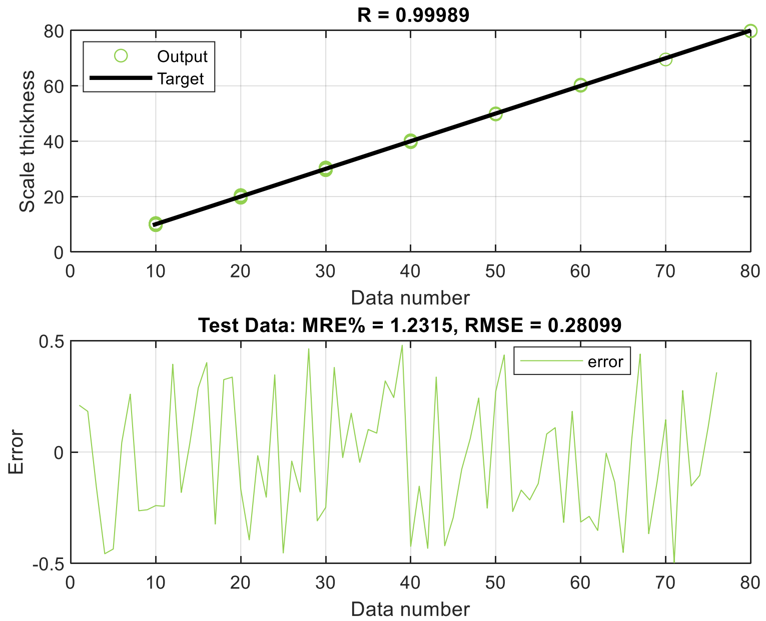

(**b**)

Figure 6. Fit and error graph for the gas volume percentage prediction neural network's (**a**) training and (**b**) testing data.

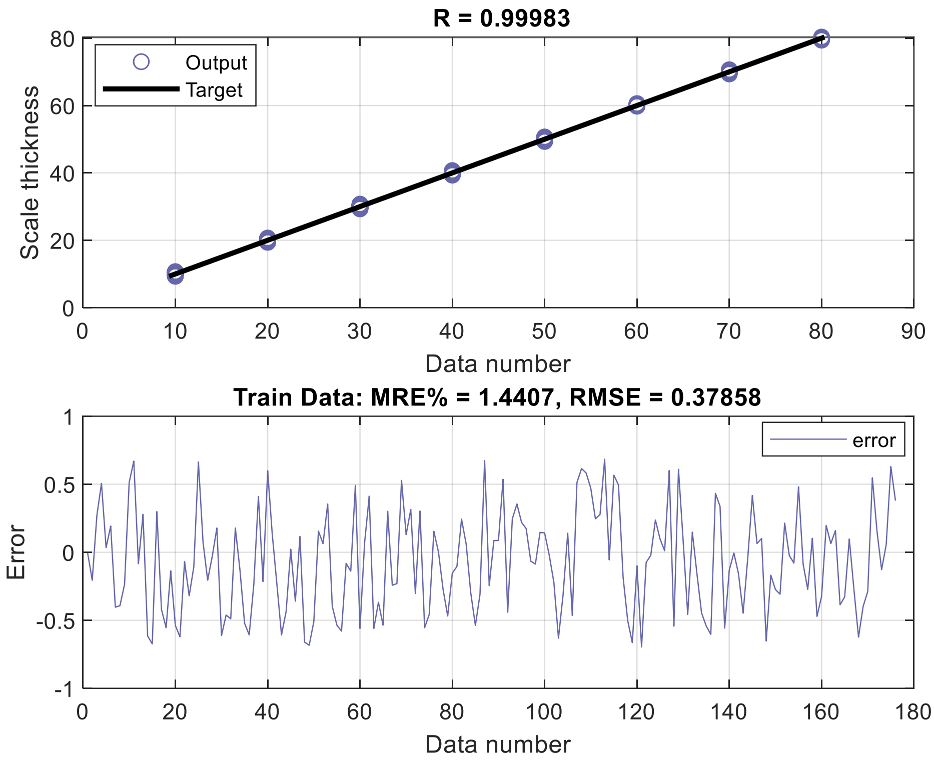

(**a**)

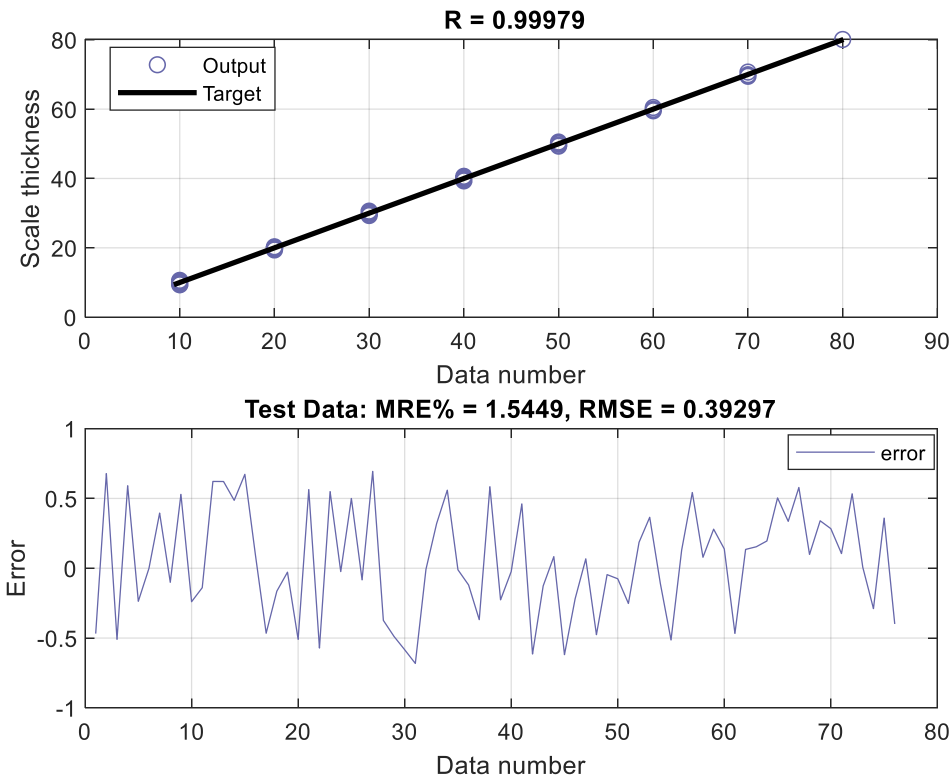

(**b**)

Figure 7. Fit and error graph for the oil volume percentage prediction neural network's (**a**) training and (**b**) testing data.

Table 2. The comparison table of the output values of the neural networks and the target.

	Oil Percentage Predictor Network				Gas Percentage Predictor Network			
	Train		Test		Train		Test	
	Output	**Target**	**Output**	**Target**	**Output**	**Target**	**Output**	**Target**
1	40.0054	40	10.4679	10	29.7982	30	9.7902	10
2	60.2055	60	29.3219	30	49.5464	50	9.8175	10
3	29.7308	30	50.5092	50	20.0054	20	10.1537	10
4	29.4942	30	19.4093	20	10.2614	10	20.4569	20
5	79.9658	80	10.2367	10	70.1311	70	60.4357	60
6	59.8074	60	50.0003	50	79.5899	80	29.9579	30
7	10.4034	10	29.6052	30	9.5809	10	19.7405	20
8	20.3924	20	20.1003	20	50.2772	50	20.2639	20
9	30.2359	30	49.4711	50	50.4051	50	10.2593	10
10	39.4869	40	30.2396	30	10.0338	10	60.2406	60
11	39.3302	40	40.1394	40	39.6092	40	30.2437	30
12	40.0838	40	9.3784	10	30.3258	30	29.6059	30
13	39.7211	40	9.3789	10	59.8381	60	10.1816	10
14	70.6152	70	59.5135	60	29.7940	30	19.9633	20
15	10.6733	10	49.3275	50	30.2463	30	49.7122	50
16	29.7013	30	9.9092	10	9.5103	10	29.5985	30
17	60.4211	60	60.4651	60	9.5484	10	60.3236	60
18	10.5546	10	10.1643	10	10.1679	10	19.6750	20
19	30.1365	30	20.0282	20	10.1035	10	49.6636	50
20	10.5376	10	10.5094	10	30.0261	30	10.1660	10
21	20.6212	20	39.4368	40	50.2297	50	10.3944	10
22	40.0688	40	40.5713	40	10.2073	10	40.0166	40
23	10.3197	10	9.4512	10	30.2814	30	40.2027	40
24	30.1075	30	10.0238	10	19.7880	20	9.6536	10
25	49.3362	50	29.5004	30	10.1925	10	30.4535	30
26	19.9251	20	80.0831	80	20.0567	20	50.0409	50
27	50.2048	50	39.3064	40	39.8965	40	10.1797	10
28	10.0297	10	40.3734	40	39.5616	40	29.5366	30
29	39.8212	40	30.4882	30	60.2802	60	10.3092	10
30	50.6120	50	30.5835	30	69.8376	70	40.2486	40
31	20.4613	20	70.6818	70	20.1079	20	19.6202	20
32	60.4887	60	30.0072	30	50.2413	50	60.0250	60
33	39.8215	40	69.6800	70	19.6048	20	39.8258	40
34	30.1305	30	9.4411	10	29.6279	30	10.0464	10
35	20.5216	20	40.0110	40	10.0495	10	9.8989	10
36	50.6069	50	30.1199	30	49.9852	50	9.9151	10
37	70.2358	70	30.3680	30	70.3905	70	79.6807	80
38	69.5895	70	29.4161	30	40.2990	40	39.7554	40

Table 2. *Cont.*

	Oil Percentage Predictor Network				Gas Percentage Predictor Network			
	Train		Test		Train		Test	
	Output	**Target**	**Output**	**Target**	**Output**	**Target**	**Output**	**Target**
39	70.2154	70	50.2262	50	30.2343	30	69.5205	70
40	79.4009	80	10.0238	10	49.5513	50	30.4237	30
41	59.8694	60	49.5395	50	49.5729	50	20.1537	20
42	50.2337	50	40.6140	40	29.5885	30	20.4326	20
43	30.6072	30	20.1267	20	20.2984	20	9.6635	10
44	30.4353	30	19.9169	20	20.4430	20	30.4211	30
45	59.9784	60	10.6187	10	80.1837	80	40.2947	40
46	10.3594	10	10.2183	10	9.6321	10	10.0774	10
47	69.8839	70	59.9327	60	20.2227	20	9.9400	10
48	30.6605	30	10.4756	10	59.6104	60	9.7576	10
49	40.6832	40	20.0457	20	9.6175	10	60.2519	60
50	50.5098	50	20.0754	20	50.1407	50	19.7287	20
51	39.8444	40	20.2521	20	9.8288	10	19.5642	20
52	29.9366	30	19.8141	20	10.1538	10	60.2673	60
53	29.6454	30	19.6350	20	40.2491	40	10.1712	10
54	10.3982	10	40.1105	40	60.0832	60	40.2152	40
55	10.5360	10	10.5136	10	40.2400	40	60.1421	60
56	20.5792	20	19.8695	20	9.7348	10	79.9190	80
57	10.0816	10	49.4577	50	20.2350	20	29.8908	30
58	70.1384	70	69.9214	70	50.4706	50	60.3161	60
59	9.5084	10	69.7203	70	10.3669	10	9.8174	10
60	20.5596	20	39.8619	40	19.5862	20	10.3145	10
61	9.9306	10	40.4667	40	9.8664	10	20.2891	20
62	49.5879	50	19.8651	20	29.8692	30	10.3523	10
63	10.5595	10	59.8462	60	70.1850	70	10.0056	10
64	20.3676	20	39.8046	40	20.0979	20	30.1357	30
65	10.5355	10	39.4964	40	50.2894	50	20.4509	20
66	9.6989	10	9.6642	10	39.8677	40	19.9440	20
67	20.2425	20	19.4215	20	49.7060	50	29.5600	30
68	40.2300	40	9.9012	10	39.5867	40	30.3667	30
69	39.4719	40	39.6602	40	20.2719	20	10.1312	10
70	19.8702	20	9.7166	10	69.7057	70	9.8551	10
71	49.6854	50	19.8948	20	29.8883	30	20.4970	20
72	30.3033	30	69.4669	70	40.0518	40	39.7242	40
73	9.6967	10	19.9931	20	39.7290	40	10.1525	10
74	60.5547	60	20.2890	20	20.1419	20	40.1050	40
75	50.4572	50	59.6410	60	69.9845	70	29.8872	30
76	19.8460	20	40.3991	40	9.6518	10	39.6422	40

Table 2. *Cont.*

	Oil Percentage Predictor Network				Gas Percentage Predictor Network			
	Train		Test		Train		Test	
	Output	Target	Output	Target	Output	Target	Output	Target
77	79.9971	80	-	-	30.2819	30	-	-
78	30.2727	30	-	-	19.6006	20	-	-
79	50.4681	50	-	-	29.7941	30	-	-
80	60.1535	60	-	-	19.7374	20	-	-
81	80.1046	80	-	-	40.0309	40	-	-
82	29.7565	30	-	-	9.5915	10	-	-
83	19.9390	20	-	-	59.9053	60	-	-
84	60.2993	60	-	-	29.6048	30	-	-
85	10.5382	10	-	-	29.6123	30	-	-
86	60.3092	60	-	-	20.2844	20	-	-
87	29.3261	30	-	-	9.7916	10	-	-
88	50.2447	50	-	-	40.1035	40	-	-
89	39.9139	40	-	-	50.4644	50	-	-
90	59.9129	60	-	-	9.9325	10	-	-
91	19.4639	20	-	-	40.1948	40	-	-
92	50.4406	50	-	-	20.2581	20	-	-
93	39.7548	40	-	-	19.9326	20	-	-
94	19.6447	20	-	-	30.1555	30	-	-
95	29.7798	30	-	-	39.6098	40	-	-
96	19.8260	20	-	-	30.4338	30	-	-
97	50.0652	50	-	-	29.6875	30	-	-
98	20.0867	20	-	-	29.7662	30	-	-
99	39.8542	40	-	-	40.2978	40	-	-
100	19.8574	20	-	-	49.9876	50	-	-
101	10.0215	10	-	-	60.2690	60	-	-
102	10.2205	10	-	-	19.8960	20	-	-
103	20.6313	20	-	-	19.7729	20	-	-
104	80.3113	80	-	-	19.5372	20	-	-
105	59.8601	60	-	-	60.1733	60	-	-
106	40.4646	40	-	-	29.9296	30	-	-
107	69.4881	70	-	-	9.9517	10	-	-
108	9.3847	10	-	-	20.1099	20	-	-
109	19.4179	20	-	-	39.5594	40	-	-
110	49.5295	50	-	-	69.8158	70	-	-
111	79.7539	80	-	-	80.2727	80	-	-
112	9.7224	10	-	-	40.1964	40	-	-
113	9.3164	10	-	-	49.6253	50	-	-
114	10.0559	10	-	-	29.6302	30	-	-

Table 2. *Cont.*

	Oil Percentage Predictor Network				Gas Percentage Predictor Network			
	Train		Test		Train		Test	
	Output	Target	Output	Target	Output	Target	Output	Target
115	19.4335	20	-	-	9.5924	10	-	-
116	19.5051	20	-	-	29.5078	30	-	-
117	20.1836	20	-	-	49.9231	50	-	-
118	10.5030	10	-	-	20.1556	20	-	-
119	30.6639	30	-	-	50.2229	50	-	-
120	20.0992	20	-	-	20.0312	20	-	-
121	30.6956	30	-	-	49.6088	50	-	-
122	30.0750	30	-	-	20.1318	20	-	-
123	20.0216	20	-	-	19.6265	20	-	-
124	9.7630	10	-	-	59.6343	60	-	-
125	19.9020	20	-	-	9.5986	10	-	-
126	29.9885	30	-	-	49.6420	50	-	-
127	49.3995	50	-	-	49.6683	50	-	-
128	30.5428	30	-	-	19.6962	20	-	-
129	29.3905	30	-	-	39.8175	40	-	-
130	29.9107	30	-	-	49.8164	50	-	-
131	40.4573	40	-	-	9.7176	10	-	-
132	49.8523	50	-	-	39.7510	40	-	-
133	30.1589	30	-	-	30.3929	30	-	-
134	20.4461	20	-	-	30.2032	30	-	-
135	10.5407	10	-	-	10.0557	10	-	-
136	30.6036	30	-	-	39.6844	40	-	-
137	39.5671	40	-	-	69.7120	70	-	-
138	49.6620	50	-	-	29.5773	30	-	-
139	30.5570	30	-	-	80.4138	80	-	-
140	40.1307	40	-	-	20.2067	20	-	-
141	60.0054	60	-	-	10.0578	10	-	-
142	10.1579	10	-	-	69.8134	70	-	-
143	70.4472	70	-	-	29.6662	30	-	-
144	50.0446	50	-	-	20.1225	20	-	-
145	9.5829	10	-	-	50.4879	50	-	-
146	9.9355	10	-	-	69.6704	70	-	-
147	9.8991	10	-	-	39.7578	40	-	-
148	10.6525	10	-	-	29.8968	30	-	-
149	10.1681	10	-	-	69.5740	70	-	-
150	20.2735	20	-	-	10.1841	10	-	-
151	60.3082	60	-	-	49.9024	50	-	-
152	39.7857	40	-	-	30.4828	30	-	-

Table 2. *Cont.*

	Oil Percentage Predictor Network				Gas Percentage Predictor Network			
	Train		Test		Train		Test	
	Output	Target	Output	Target	Output	Target	Output	Target
153	10.0238	10	-	-	19.9022	20	-	-
154	60.0794	60	-	-	30.1207	30	-	-
155	39.5191	40	-	-	69.6544	70	-	-
156	30.0869	30	-	-	19.8813	20	-	-
157	20.2727	20	-	-	19.6611	20	-	-
158	9.8970	10	-	-	20.2581	20	-	-
159	20.4708	20	-	-	20.3711	20	-	-
160	30.3239	30	-	-	59.8508	60	-	-
161	49.8040	50	-	-	60.1855	60	-	-
162	9.9359	10	-	-	39.7941	40	-	-
163	29.8409	30	-	-	60.0306	60	-	-
164	30.3858	30	-	-	60.3324	60	-	-
165	10.3280	10	-	-	50.0975	50	-	-
166	49.9024	50	-	-	39.8353	40	-	-
167	20.2713	20	-	-	79.7992	80	-	-
168	50.6233	50	-	-	59.9526	60	-	-
169	20.3979	20	-	-	69.9226	70	-	-
170	20.2878	20	-	-	19.8596	20	-	-
171	29.4531	30	-	-	40.0583	40	-	-
172	9.8459	10	-	-	10.2425	10	-	-
173	60.1273	60	-	-	9.9243	10	-	-
174	9.9431	10	-	-	9.9294	10	-	-
175	69.3705	70	-	-	39.6249	40	-	-
176	19.6202	20	-	-	49.5244	50	-	-

Table 3. Evaluation of the suggested detection method's accuracy in light of existing research.

Ref.	Maximum MSE	Maximum RMSE	Extracted Features	Type of Neural Network
[5]	0.21	0.46	Time features	MLP
[27]	7.34	2.71	No feature extraction	GMDH
[28]	1.24	1.11	Time features	GMDH
[29]	0.67	0.82	Frequency features	MLP
[30]	2.56	1.6	No feature extraction	MLP
[31]	1.08	1.04	No feature extraction	MLP
[32]	0.19	0.44	Wavelet features	GMDH
[current study]	0.07	0.27	Frequency features	RBF

This study has the potential benefit of reducing the number of computations used by the system. By constructing neural networks that capitalize on the best features of the input data, we could decrease the amount of computations required. In less than 5 min, the computer system (Processor Intel(R) Core i7-10750H, RAM16GB, Graphics Card GeForce GTX 1650 Ti) completed the computations necessary for feature extraction and neural network building. In the current investigation, the fundamental limitation is the incorporation of radiation sources into the structural layout of the detecting equipment. Because of the dangers posed by radiation, special protective gear is required whenever this machinery is used. Since the source cannot be switched off, however, transporting such devices presents significant logistical challenges and necessitates the use of specialist radiation-limiting gear. In order to solve this problem, in future researchers can work on the use of X-ray-based flowmeters, capacitance-based and even resistance-based flowmeters so that they can avoid the harmful effects of using radioisotopes. The low error rate attained in this study is a consequence of correctly processing the signals that were acquired and training the neural network using the signal's useful properties that can mask flaws. This tiny inaccuracy allowed for highly accurate volume percentage predictions when scale was present. Researchers in the oil field should pay close attention to investigating additional features of the received signals and studying the extracted features with optimization-based feature selection techniques, in light of the importance of feature extraction in identifying the parameters of the oil field.

4. Conclusions

The system will be optimized, and the oil industry's performance will increase, by knowing the volume percentage of each condensate phase that passes within the oil pipe. Consequently, developing and putting in place a system to identify volume percentage can be a useful aid in resolving problems in the oil industry. In this work, the most precise approach in order to determine the volume percentage of three-phase condensates flowing in a stratified flow pattern was developed using the gamma-ray attenuation method. A dual energy gamma source and two NaI detectors positioned on either side of the pipe make up the detection system, which measures the volume percentage of each phase. MCNP code is used to mimic every step of this process. While examining various scale values, a three-phase flow was simulated at various volume percentages. Four characteristics were retrieved from the signals from all simulations and employed in the building of neural networks. These features were the amplitude of the first and second dominant frequency of signals received by both detectors. The above-mentioned characteristics were taken into account as inputs for two RBF neural networks, and each network's output was the volume percentage of gas and oil. By deducting the amount of oil and gas from the overall volume of the pipe, the volume percentage of the water phase may be easily calculated. In comparison to other studies, this neural network's prediction of the volume percentage has an RMSE of less than 0.29, which is a small error. Oil, gas, and petrochemical industries that deal with multi-phase flows and the need to accurately and in real-time determine the volume of each phase can use the methodology presented in this research to determine the desired parameters.

Author Contributions: Conceptualization, A.M.M., J.W.G.G., T.I., J.K.B., N.K.S., E.E.-Z. and H.H.A.; Software, A.M.M., J.W.G.G., T.I., J.K.B., N.K.S. and H.H.A.; Investigation, A.M.M., J.W.G.G., T.I., J.K.B., N.K.S., E.E.-Z. and H.H.A.; Writing—original draft, A.M.M., J.W.G.G., T.I., J.K.B. and H.H.A. All authors have read and agreed to the published version of the manuscript.

Funding: The authors extend their appreciation to the Deanship of Scientific Research at King Khalid University for funding this work through large group Research Project under grant number RGP2/39/44. We acknowledge support by the German Research Foundation Projekt-Nr. 512648189 and the Open Access Publication Fund of the Thueringer Universitaets- und Landesbibliothek Jena.

Data Availability Statement: The data presented in this study are available on request from the corresponding author.

Conflicts of Interest: The authors declare no conflict of interest.

References

1. Nazemi, E.; Roshani, G.H.; Feghhi, S.A.H.; Setayeshi, S.; Zadeh, E.E.; Fatehi, A. Optimization of a method for identifying the flow regime and measuring void fraction in a broad beam gamma-ray attenuation technique. *Int. J. Hydrogen Energy* **2016**, *41*, 7438–7444. [CrossRef]

2. Mayet, A.M.; Alizadeh, S.M.; Hamakarim, K.M.; Al-Qahtani, A.A.; Abdullah, K.; Guerrero, J.W.G.A.; Hala, H.A.; Eftekhari-Zadeh, E. Application of Wavelet Characteristics and GMDH Neural Networks for Precise Estimation of Oil Product Types and Volume Fractions. *Symmetry* **2022**, *14*, 1797. [CrossRef]
3. Islamirad, S.Z.; Gholipour Peyvandi, R. Precise volume fraction measurement for three-phase flow meter using 137Cs gamma source and one detector. *Radiochim. Acta* **2020**, *108*, 159–164. [CrossRef]
4. Rad, I.; Zahra, S.; Peyvandi, R.G.; Gharaghani, H.P. Evaluation of nuclear data analysis techniques for volume fraction prediction in the flow meter. *Radiochim. Acta* **2023**, *111*, 73–79.
5. Sattari, A.M.; Roshani, G.H.; Hanus, R. Improving the structure of two-phase flow meter using feature extraction and GMDH neural network. *Radiat. Phys. Chem.* **2020**, *171*, 108725. [CrossRef]
6. ShadSanjabad, M.; Feghhi, A.; Ghaderi, R. Regime independent flow rate prediction in a gas-liquid two-phase facility based on gamma ray technique and one detector using multi-feature extraction. *Flow Meas. Instrum.* **2023**, *92*, 102388. [CrossRef]
7. Tzu-Chia, C.; Abdullah, M.; Hanus, I.R.; Salama, A.S.; Hirota, K. Predicting Scale Thickness in Oil Pipelines Using Frequency Characteristics and an Artificial Neural Network in a Stratified Flow Regime. *Energies* **2022**, *15*, 7564.
8. Salgado, C.M.; Brandão, L.E.B.; Pereira, C.M.N.A.; Salgado, W.L. Salinity independent volume fraction prediction in annular and stratified (water–gas–oil) multiphase flows using artificial neural networks. *Prog. Nucl. Energy* **2014**, *76*, 17–23. [CrossRef]
9. Jeshvaghani, P.; Rezaee, A.K.; Feghhi, S.A.H.; Jafari, A. Using statistical features and a neural network to predict gas volume fractions independent of flow regime changes. *Flow Meas. Instrum.* **2023**, *93*, 102430. [CrossRef]
10. Hossein, R.G.; Ali, P.J.M.; Mohammed, S.; Hanus, R.; Abdulkareem, L.; Alanezi, A.A.; Sattari, M.A.; Amiri, S.; Nazemi, E.; Eftekhari-Zadeh, E.; et al. Simulation study of utilizing X-ray tube in monitoring systems of liquid petroleum products. *Processes* **2021**, *9*, 828.
11. Mohammed, B.; Sattari, M.A.; Taylan, O.; Bakhsh, A.A.; Nazemi, E. Applications of discrete wavelet transform for feature extraction to increase the accuracy of monitoring systems of liquid petroleum products. *Mathematics* **2021**, *24*, 3215.
12. Tzu-Chia, C.; Abdullah, M.; Alizadeh, I.S.M.; Ahmed, S.; Eftekhari-Zadeh, S.E.; Hirota, K. The use of artificial intelligence and time characteristics in the optimization of the structure of the volumetric percentage detection system independent of the scale value inside the pipe. *Appl. Artif. Intell.* **2023**, *37*, 2166225.
13. Marques, S.C.; de Freitas Dam, R.S.; de Carvalho Conti, C.; Salgado, W.L. Three-phase flow meters based on X-rays and artificial neural network to measure the flow compositions. *Flow Meas. Instrum.* **2021**, *82*, 102075.
14. Eng, L.A.; Goh, S. Effect of microchannel diameter on electroosmotic flow hysteresis. *Energies* **2023**, *16*, 2154.
15. Serov, V.; John, T.M.; Hoogenboom, J.E. A new effective Monte Carlo Midway coupling method in MCNP applied to a well logging problem. *Appl. Radiat. Isot.* **1998**, *49*, 1737–1744. [CrossRef]
16. Juntao, L.; Zhang, F.; Wang, X.; Han, F.; Yuan, Z. Numerical study on determining formation porosity using a boron capture gamma ray technique and MCNP. *Appl. Radiat. Isot.* **2014**, *94*, 266–271.
17. Effendy, N.; Zaid, M.H.M.; Sidek, H.A.A.; Matori, K.A.; Mahmoud, K.A.; Sayyed, M.I. Influence of ZnO to the physical, elastic and gamma radiation shielding properties of the tellurite glass system using MCNP-5 simulation code. *Radiat. Phys. Chem.* **2021**, *188*, 109665. [CrossRef]
18. Ozan, T.H.; Manici, T. Simulations of mass attenuation coefficients for shielding materials using the MCNP-X code. *Nucl. Sci. Tech.* **2017**, *28*, 95.
19. Pelowitz, D.B. *MCNP-X TM User's Manual*; Version 2.5.0, LA-CP-05e0369; Los Alamos National Laboratory: Los Alamos, NM, USA, 2005.
20. Nussbaumer, H.J. *The Fast Fourier Transform*; Springer: Berlin/Heidelberg, Germany, 1981.
21. Yu, B.; He, X. Training radial basis function networks with differential evolution. *IEEE Int. Conf. Granul. Comput.* **2006**, *11*, 369–372. [CrossRef]
22. Hartman, E.J.; Keeler, J.D.; Kowalski, J.M. Layered neural networks with Gaussian hidden units as universal approximators. *Neural Comput.* **1990**, *2*, 210–215. [CrossRef]
23. Al-Naser, M.; Elshafei, M.; Al-Sarkhi, A. Artificial neural network application for multiphase flow patterns detection: A new approach. *J. Pet. Sci. Eng.* **2016**, *145*, 548–564. [CrossRef]
24. Świsulski, D.M. Uncertainty of mass flow measurement using centric and eccentric orifice for Reynolds number in the range $10{,}000 \leq Re \leq 20{,}000$. *Measurement* **2020**, *160*, 107851.
25. Yan, Y.; Wang, L.; Wang, T.; Wang, X.; Hu, Y.; Duan, Q. Application of soft computing techniques to multiphase flow measurement: A review. *Flow Meas. Instrum.* **2018**, *60*, 30–34. [CrossRef]
26. Mohammad, M.A.; Chen, T.-C.; Alizadeh, S.M.; Al-Qahtani, A.A.; Qaisi, R.M.A.; Alhashim, H.H.; Eftekhari-Zadeh, E. Application of Artificial Intelligence for Determining the Volume Percentages of a Stratified Regime's Three-Phase Flow, Independent of the Oil Pipeline's Scale Thickness. *Processes* **1996**, *10*, 10.
27. Mohammadmehdi, R.; Sattari, M.A.; Ali, P.J.M.; Roshani, G.H.; Nazemi, B.; Corniani, E.; Nazemi, E. Application of GMDH neural network technique to improve measuring precision of a simplified photon attenuation based two-phase flowmeter. *Flow Meas. Instrum.* **2020**, *75*, 101804.
28. Amir, S.M.; Roshani, G.H.; Hanus, R.; Nazemi, E. Applicability of time-domain feature extraction methods and artificial intelligence in two-phase flow meters based on gamma-ray absorption technique. *Measurement* **2021**, *168*, 108474. [CrossRef]

29. Hosseini, S.; Roshani, G.H.; Setayesh, S. Precise gamma based two-phase flow meter using frequency feature extraction and only one detector. *Flow Meas. Instrum.* **2020**, *72*, 101693. [CrossRef]
30. Gholipour, P.R.; Islami Rad, S.Z. Application of artificial neural networks for the prediction of volume fraction using spectra of gamma rays backscattered by three-phase flows. *Eur. Phys. J. Plus* **2017**, *132*, 511. [CrossRef]
31. Roshani, G.H.; Nazemi, E.; Feghhi, S.A.H.; Setayeshi, S. Flow regime identification and void fraction prediction in two-phase flows based on gamma ray attenuation. *Measurement* **2015**, *62*, 25–32. [CrossRef]
32. Mayet, A.M.; Alizadeh, S.M.; Kakarash, Z.A.; Al-Qahtani, A.A.; Alanazi, A.K.; Alhashimi, H.H.; Eftekhari-Zadeh, E.; Nazemi, E. Introducing a precise system for determining volume percentages independent of scale thickness and type of flow regime. *Mathematics* **2020**, *10*, 1770. [CrossRef]